© 2014. Published by The Company of Biologists Ltd | Development (2014) 141, 4168-4181 doi:10.1242/dev.109918

RESEARCH ARTICLE

Arid3b is essential for second heart field cell deployment and heart patterning

Verónica Uribe[1], Claudio Badía-Careaga[1], Jesús C. Casanova[1,*], Jorge N. Domínguez[3], José Luis de la Pompa[1] and Juan José Sanz-Ezquerro[1,2,‡]

ABSTRACT

Arid3b, a member of the conserved ARID family of transcription factors, is essential for mouse embryonic development but its precise roles are poorly understood. Here, we show that *Arid3b* is expressed in the myocardium of the tubular heart and in second heart field progenitors. *Arid3b*-deficient embryos show cardiac abnormalities, including a notable shortening of the poles, absence of myocardial differentiation and altered patterning of the atrioventricular canal, which also lacks epithelial-to-mesenchymal transition. Proliferation and death of progenitors as well as early patterning of the heart appear normal. However, DiI labelling of second heart field progenitors revealed a defect in the addition of cells to the heart. RNA microarray analysis uncovered a set of differentially expressed genes in *Arid3b*-deficient tissues, including *Bhlhb2*, a regulator of cardiomyocyte differentiation, and *Lims2*, a gene involved in cell migration. *Arid3b* is thus required for heart development by regulating the motility and differentiation of heart progenitors. These findings identify *Arid3b* as a candidate gene involved in the aetiology of human congenital malformations.

KEY WORDS: Heart development, *Arid3b*, Second heart field, Transcription factor, DiI labelling, AVC explant, Cell motility, Mouse

INTRODUCTION

Understanding heart development (Vincent and Buckingham, 2010; Bruneau, 2013; Miquerol and Kelly, 2013; Rana et al., 2013) is important for identifying the origin of congenital heart malformations, the most common birth defects (Fahed et al., 2013). The heart develops from two populations of cardiac progenitors (Buckingham et al., 2005). The initial heart tube (which will form the left ventricle) originates from cardiogenic mesodermal cells, which fuse at the ventral midline of the embryo. Elongation of the heart is driven by the addition at the poles of a second pool of Islet1+ (Isl1 – Mouse Genome Informatics) progenitor cells located in the pharyngeal mesoderm beneath the heart tube and called the second heart field (SHF) (Kelly, 2012). As these progenitors get incorporated into the heart poles, they differentiate and start to express myocardium markers, such as smooth muscle actin (SMA) and TroponinT (TnT). Cells from the SHF contribute to the outflow tract (OFT), right ventricle, atrioventricular canal (AVC), atria and the inflow tract (IFT). Multiple signalling pathways are implicated in regulating the proliferation and differentiation of the SHF population (Black, 2007; Rochais et al., 2009); however, little is known about the cellular mechanisms that drive the deployment of SHF cells to the heart poles. Chick dye labelling showed that cells from a caudal proliferative centre are able to move to the arterial pole (van den Berg et al., 2009). Cardiogenic mesoderm in this region in the chick is reported to be a cohesive epithelial sheet possessing a columnar pseudostratified structure (Waldo et al., 2005). Recently, Wnt5a-activated PCP signalling in the mouse has been proposed to induce a mesenchymal-to-epithelial conversion of splanchnic mesoderm, promoting SHF contribution to the OFT through a process of cell intercalation (Sinha et al., 2012).

The AVC separates the ventricle from the atria, and cells in this area are distinguished from atrial and ventricular neighbours by a distinct molecular code. The AVC is also characterized by the expression of *Bmp2*, which signals to the endocardium and promotes epithelial-to-mesenchymal transition (EMT) (Sugi et al., 2004; Ma et al., 2005), generating the AVC cushions that will subsequently form the valves that separate the chambers (von Gise and Pu, 2012). Bmp2 directly regulates myocardial expression of *Tbx2*, which, together with *Tbx3*, is expressed in the AVC and represses the expression of chamber-specific genes, including *Anf* (*Nppa* – Mouse Genome Informatics) and *Cx40* (*Gja5* – Mouse Genome Informatics) (Singh et al., 2009, 2012).

The Arid family is a conserved group of genes characterized by the presence of a distinctive DNA-binding domain, the AT-rich interacting domain ARID (Kortschak et al., 2000; Wilsker et al., 2005). Members of this family play important roles in the regulation of cell cycle, gene expression, development and differentiation (Shandala et al., 2002; Wilsker et al., 2002). ARID proteins seem to function as transcriptional regulators in multiprotein complexes, acting as context-dependent activators or repressors (Valentine et al., 1998) and also participate in chromatin-remodelling activities as part of the SWI/SNF and polycomb repressor complexes (Nagl et al., 2007; Peng et al., 2009).

Arid3b (also known as *Bdp* or *Dri2*) was first cloned in a two-hybrid screen as a binding partner of retinoblastoma protein (Numata et al., 1999). *Arid3b* is expressed in different types of cancers, including malignant neuroblastomas. It can transform mouse embryonic fibroblasts and, together with *Mycn*, forms a combination with strong oncogenic activity (Kobayashi et al., 2006); in mouse embryonic stem cells (ESCs) these two genes are involved in cell proliferation (Kobayashi et al., 2013). *Arid3b* is overexpressed in malignant ovarian cancers and is involved in the mesenchymal transformation of ovarian epithelial cells (Cowden Dahl et al., 2009). Transient silencing of *Arid3b* in breast cancer cells decreases cell migration, implicating *Arid3b* as a miR-125b target with roles in cell motility (Akhavantabasi et al., 2012). *Arid3b*

[1]Departamento de Desarrollo y Reparación Cardiovascular, Centro Nacional de Investigaciones Cardiovasculares (CNIC), Melchor Fernández Almagro, 3, Madrid 28029, Spain. [2]Departamento de Biología Molecular y Celular, Centro Nacional de Biotecnología (CSIC), Darwin, 3, Madrid 28049, Spain. [3]Departamento de Biología Experimental, Facultad de Ciencias Experimentales, Universidad de Jaén, CU Las Lagunillas, Jáen 23071, Spain.
*Present address: Australian Regenerative Medicine Institute, ARMI, Monash University, Clayton, Australia.

‡Author for correspondence (jjsanz@cnb.csic.es)

Received 10 March 2014; Accepted 31 August 2014

Development (2014) 141, 4168-4181 doi:10.1242/dev.109918

is also essential for embryonic development. *Arid3b* mutants die at mid-gestation, showing severe craniofacial and cardiovascular defects (Takebe et al., 2006), although a role for *Arid3b* in heart development has been dismissed. We have shown that *Arid3b* contributes to the proper maturation of the limb apical ectodermal ridge in both chick and mouse embryos by controlling cell rearrangements, as well as being necessary for proper motility of mouse embryonic fibroblasts (MEFs) *in vitro* (Casanova et al., 2011). However, the specific roles of this gene remain elusive.

Here, we show that *Arid3b* is dynamically expressed in the developing embryonic heart. Absence of *Arid3b* leads to failed deployment of cells from the SHF to both heart poles and to defective patterning of the AVC and disruption of EMT in the endocardial cushions. Microarray analysis reveals upregulation of *Lims2* and *Bhlhb2* (*Bhlhe40* – Mouse Genome Informatics) as candidate mediators of *Arid3b* function in regulating cell movements and differentiation of SHF cardiac progenitors.

RESULTS

Arid3b is expressed in the heart from early stages of development

Arid3b is essential during embryonic development and mouse embryos lacking *Arid3b* die at mid-gestation (Takebe et al., 2006; Casanova et al., 2011). As the possible role of *Arid3b* in heart development has not been fully investigated, we first analysed its expression pattern by RNA *in situ* hybridisation. *Arid3b* is expressed from early stages in the heart crescent (Fig. 1A). At E8.0, expression is observed throughout the primary heart tube myocardium and also strongly in the SHF (Fig. 1B-D; supplementary material Fig. S1). At E8.5, expression in the heart tube is fainter but remains strong in the SHF and the heart poles (Fig. 1E; supplementary material Fig. S1). At E9.0, high-level expression persists in the heart poles (IFT and OFT) and in the SHF (Fig. 1F-J; supplementary material Fig. S1). However, expression gradually decreases in the heart chambers, whereas it is clearly observed in the AVC (Fig. 1I). At E9.5, expression is still strong in the sinus venosus, dorsal mesocardium and OFT (Fig. 1K-O). At E10.5, expression in the heart myocardium is much fainter, but a clear signal is still seen in the OFT (Fig. 1P,Q). From E11 onwards, expression in the myocardium is no longer detected. *Arid3b* is also expressed from E10.5 in the endocardium and between E11.5 and E12.5 there is an especially strong signal in the endocardium of the AVC and OFT (Fig. 1R-U). At E14.5, strong expression is detected in the arterial trunk (Fig. 1V). Expression is also present in the epicardium at these stages (Fig. 1R,T). In blood vessels, *Arid3b* is not expressed in the endothelium at early stages, although expression is high in the yolk sac endoderm (supplementary material Fig. S2). However, from E9.5, expression is readily seen in the vessel endothelium (Fig. 1X). This expression is first seen in the aorta and large vessels, including veins, and later extends to smaller vessels (Fig. 1V-X).

Arid3b null embryos show cardiac defects

To analyse the role of *Arid3b* in heart development we have used a mouse gene trap line in which *Arid3b* lacks its functional domains (Casanova et al., 2011). Embryos deficient for *Arid3b* (*Arid3b*$^{gt/gt}$) die at E10.5 and show reduced size, arrest in somitogenesis and severe craniofacial and cardiovascular malformations, including an abnormally dilated heart with altered looping and pericardial effusion (Fig. 2A,B). Moreover, the yolk sac lacks large mature blood vessels, suggesting that appropriate vascular remodelling is impaired (Fig. 2C). However, mutant hearts beat and Indian Ink distributes to the body after injection into the heart at E9.25, confirming blood circulation (Fig. 2J,O). Closer examination of the mutant hearts reveals a shortening of the OFT and IFT at E8.5 (Fig. 2D,E) and E9.0 (Fig. 2F,G,K,L), which becomes more evident at E9.5 (Fig. 2H,I,M,N; supplementary material Fig. S3 shows a quantitative comparison of the lengths). In histological sections at E9.5, the mutant heart shows disorganized sinus horns, thinner myocardium walls in atria and the ventricle, and reduced trabeculation compared with the wild-type (WT) heart (Fig. 2P-S,U-X). Moreover, the mutant OFT is short and the AVC is narrow and does not show the EMT of the endocardium that is already evident in WT hearts (Fig. 2R,W). Transformed mesenchymal cells cannot be detected in the OFT cushion either, suggesting a general defect in EMT (supplementary material Fig. S4). The expression pattern of *Arid3b* and the early heart defects in the mutant embryos suggest that *Arid3b* is directly required for proper heart morphogenesis.

Arid3b is required for AVC patterning and EMT

To evaluate whether *Arid3b* deletion affects genes known to be important for heart formation, we performed *in situ* hybridisation to detect mRNA expression of cardiac transcription factors, signalling molecules and myofiber genes. Wild-type and mutant hearts showed similar patterns and levels of expression at E9.0 for *Nkx2-5* and *Gata4* (two early cardiac master genes). Normal expression was also detected for the key cardiac transcription factors and chamber-specific markers *Mef2c*, *Tbx5*, *Mlc2v* (*Myl2* – Mouse Genome Informatics), *Hand1*, *Hand2*, *Hey1* and *Hey2* (supplementary material Fig. S5), suggesting that early patterning of the heart is not affected in *Arid3b*$^{gt/gt}$ mutants.

An important heart region affected in the mutant is the AVC. Expression of *Bmp2*, an upstream regulator of AVC patterning (Rutenberg et al., 2006), was the same in mutant and WT hearts at E9.0 (Fig. 3A). However, *Arid3b* null hearts showed significantly below-normal expression of *Tbx2* and *Tbx3*, targets of BMP signalling and determinants of AVC specification through the repression of chamber-specific genes (Fig. 3A). Notably, expression of the chamber myocardium marker *Anf* was expanded to the AVC region (Fig. 3A), suggesting the loss of AVC patterning. These altered expression patterns persisted at E9.5 (Fig. 3B), but were now accompanied by a significant drop in the expression of *Bmp2*, as detected by *in situ* hybridisation (Fig. 3B) and quantitative PCR (supplementary material Fig. S6A). This indicates disruption of the regulatory-feedback loop between *Bmp2*, *Tbx2* and *Tbx3*, thus impairing the maintenance of AVC identity. This result was confirmed by analysis of the chamber markers *Cx40* and *Cx43* (*Gja1* – Mouse Genome Informatics), which were expanded into the mutant AVC (supplementary material Fig. S7). To characterize the origin of the AVC alterations we analysed nuclear localization of pSmad, which mediates BMP signalling. In the AVC myocardium, similar nuclear localization of pSmad, indicative of pathway activation, was observed in WT and *Arid3b* null hearts at E9.0 (Fig. 3Cc,d) and E9.5 (Fig. 3Cg,h), despite the lower *Bmp2* expression in mutants at E9.5 (compare Fig. 3Ca,b with e,f). Moreover, nuclear pSmad localization was present in mutant AVC endocardium at E9.0 (Fig. 3Cc,d), whereas at E9.5 the number of pSmad-positive endocardial cells was significantly lower in mutant than in WT AVC (30% reduction, n=3; P<0.01 in Student's t-test) (Fig. 3Cg,h).

These results suggest that *Arid3b* acts in the myocardium downstream of pSmad nuclear translocation and that Bmp2 signalling from the AVC myocardium is not transduced properly to the endocardium. To gain further insight into *Arid3b* function in the AVC, we analysed the expression of EMT markers (*Snai1*,

Development (2014) 141, 4168-4181 doi:10.1242/dev.109918

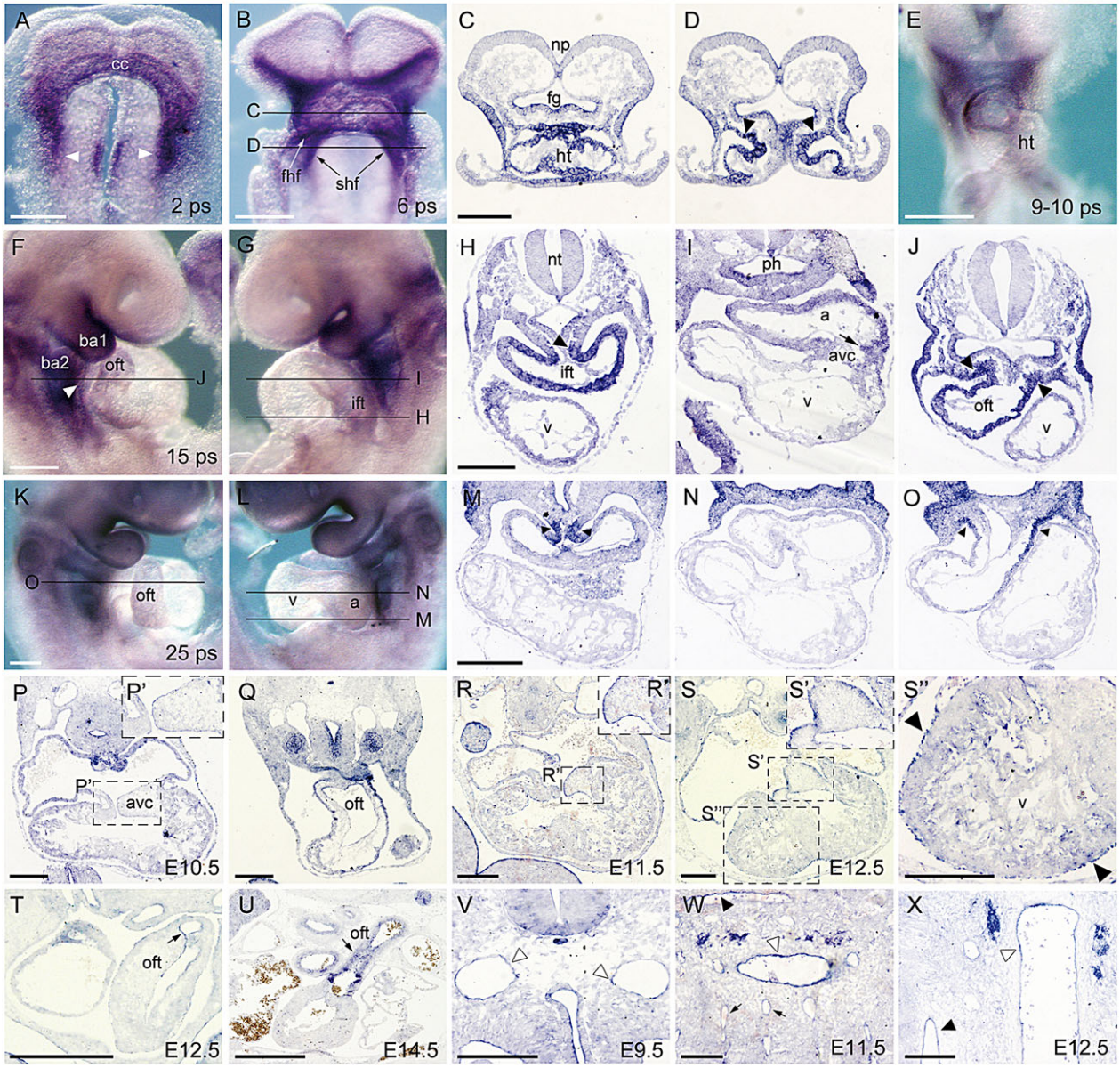

Fig. 1. *Arid3b* is expressed in the heart from early stages of development. RNA *in situ* hybridization showing *Arid3b* expression at different stages of mouse heart development in whole-mount embryos (A,B,E-G,K,L) and on paraffin sections (C,D,H-J,M-X). From early stages expression is observed throughout the heart tube and in the SHF (A-D, arrowheads). In the looping heart expression diminishes in the developing chambers (E) but is maintained strongly in the myocardium of the heart poles (oft in F,K and ift in G) and in the SHF (F-O, arrowheads in F,H,J,M,O). Expression can also be observed in the AVC myocardium at E9.0 (I, arrow), but not at E9.5. From E10.5, expression is observed in the endocardium, especially in the AVC cushions (P,P′,R,R′,S,S′,S″) and later in the OFT cushions (T,U, arrows). We also observed expression in the epicardium at E12.5 (S″, arrowheads). In the vessels *Arid3b* expression starts in the dorsal aorta at E9.5 (V,W,X, white arrowheads) and later also appears in small vessels (arrows) and in veins (black arrowheads) (W,X). Scale bars: 150 µm in C,D,H-J,M-O,V-X; 250 µm in A,B,E,F,G,K,L,P-S″; 500 µm in T,U. Stages are indicated as embryonic day (e.g. E10.5) or pairs of somites, ps. a, atrium; ba, branchial arches; cc, cardiac crescent; fg, foregut; fhf, first heart field; ht, heart tube; ift, inflow tract; np, neural plate; nt, neural tube; oft, outflow tract; ph, pharynx; shf, second heart field; v, ventricle. Lines in B,F,G,K,L mark plane of sections showed in the indicated panels.

Tgfb2, *Twist1*, *Has1* and *Tbx20*), some of which are known targets of BMP signalling. At E9.5, EMT is already detected in the WT AVC, and transformed cells expressing mesenchymal markers are observed in the cardiac jelly (Fig. 4A). By contrast, these cells are not present in *Arid3b*-deficient AVC (Fig. 4A). Moreover, although *Tgfb2* expression was detected in WT and *Arid3b*-null AVC myocardium (Fig. 4A), expression of *Snai1*, *Tgfb2*, *Twist1* and *Tbx20* were undetectable in mutant AVC endocardium (Fig. 4A).

These data show that EMT is impaired in *Arid3b* mutant hearts and suggest that the primary defect in these mutants is incorrect signalling from myocardial Bmp2 to the endocardium. To test this possibility, we cultured AVC explants on collagen gels. In these conditions, endocardial cells undergo EMT and invade the collagen gel, which can be measured and quantified as the transformation index [% invading cells/total number of transformed cells, see Materials and Methods (Luna-Zurita et al., 2010)]. Compared with WT AVC explants, mutant explants generated significantly fewer transformed cells and, more importantly, a significantly lower transformation index (Fig. 4B-D). Addition of Bmp2 to the culture medium rescued these defects, restoring the total number of transformed cells and the

Development (2014) 141, 4168-4181 doi:10.1242/dev.109918

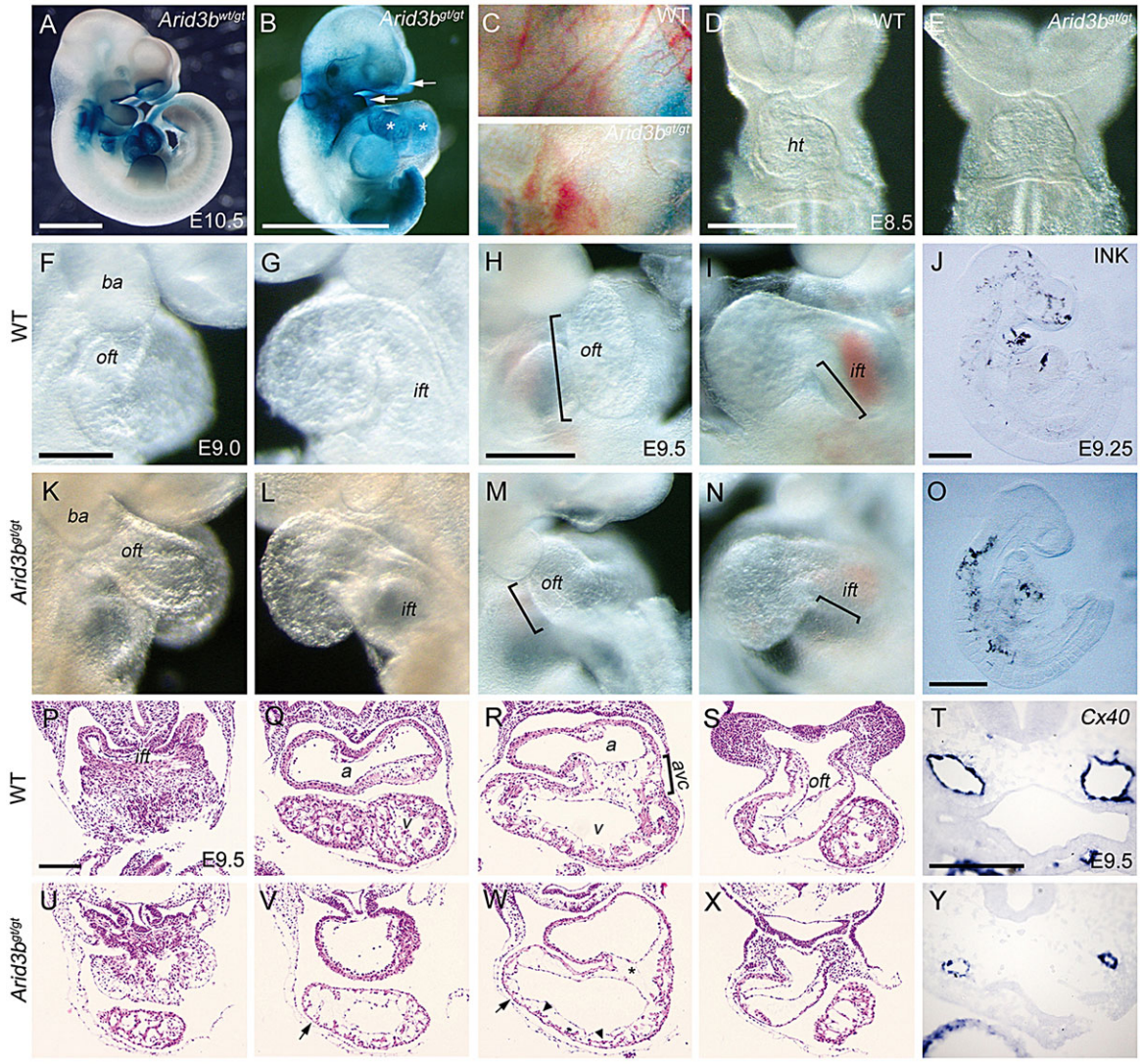

Fig. 2. *Arid3b* mutant embryos show early cardiac defects. β-gal staining of (A) *Arid3b*$^{+/gt}$ (heterozygous control) and (B) *Arid3b*$^{gt/gt}$ (homozygous mutant) embryos at E10.5. Major defects are seen in the mutant: smaller size (note the different scale) and craniofacial (arrows) and heart (asterisks) malformations. (C) Absence of normal vascular remodelling in the *Arid3b*$^{gt/gt}$ yolk sac. (D,E) Defective looping and heart pole formation is seen as early as E8.5 in *Arid3b* null embryos. (F,G,K,L) At stage E9.0, *Arid3b*$^{gt/gt}$ embryos show a substantial shortening of the OFT and IFT, which becomes more evident at E9.5 (H,I,M,N, brackets). (J,O) Injection of Indian Ink into the heart confirms blood circulation in mutant embryos, although vessels are smaller than in WT embryos, as shown by *Cx40* expression (RNA *in situ* hybridisation in T,Y). (P-S,U-X) Haematoxylin & Eosin (H&E) staining on sections of E9.5 embryos, showing abnormal heart structure in *Arid3b* null embryos. The poles appear disorganised (IFT, compare U with P; OFT, compare X with S). Note also the thinned myocardium (V,W, arrows), reduced trabeculation in the ventricle (W, arrowheads) and absence of EMT in the AVC (W, asterisk). Scale bars: 150 µm in P-X,T-Y; 250 µm in F,G, K,L; 500 µm in A,B,D,E,H-J,M-O. ba, branchial arch; all other abbreviations as in Fig. 1 legend.

transformation index to values similar to those of WT explants (Fig. 4B-D). This result confirms that the EMT deficiency in *Arid3b* mutant AVC is caused by inefficient Bmp2 signalling.

Microarray analysis identifies candidate genes and processes mediating *Arid3b* effects on heart development

To identify the genes mediating *Arid3b* function in heart development, we performed a microarray comparison of mRNA expression in WT and mutant embryos. In two separate experiments, RNA was extracted from whole E9.0 embryos or from E9.5 hearts, heads and trunks, and expression was compared between the samples using Agilent chips (Fig. 5Aa-c; supplementary material Tables S1-S4). Of the genes showing differential expression in *Arid3b*-null embryos, 93 were altered in both E9.0 whole embryos and E9.5 hearts, and 453 genes were common to the three tissues analysed in E9.5 embryos (Fig. 5Ad,e; supplementary material Tables S5, S6). Ingenuity functional analysis of the sets of common genes revealed cell morphology and cellular movement as the most highly overrepresented functions (Fig. 5B; supplementary material Table S7). These results support a role for *Arid3b* in the control of cell motility and cellular rearrangements, in agreement with a previous analysis (Casanova et al., 2011).

To validate the microarray data, we conducted mRNA *in situ* hybridisation analysis of genes showing high differential expression and which have established roles in embryonic development (Fig. 5C; supplementary material Fig. S8). Selected genes included members of important signalling pathways and genes involved in vessel or muscle differentiation. Clear up- or downregulation of these genes was observed, in agreement with the microarray result. For more in-depth analysis, we focused on two upregulated genes that could provide

Development (2014) 141, 4168-4181 doi:10.1242/dev.109918

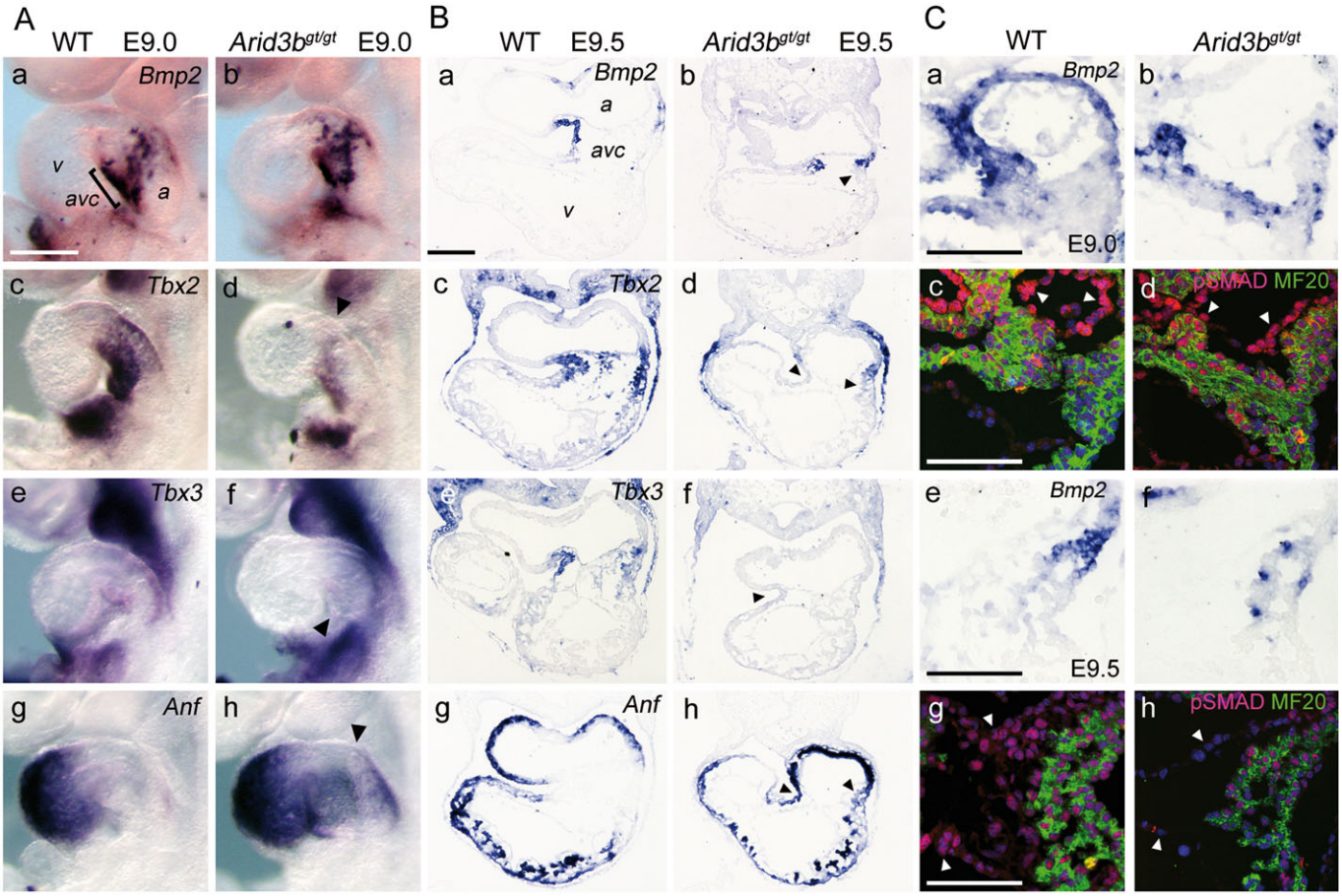

Fig. 3. *Arid3b* is required for patterning of the AVC. (A) *In situ* hybridisation of molecules important for AVC patterning at E9.0 (whole-mount). *Bmp2* expression (a,b) in E9.0 *Arid3b*$^{gt/gt}$ embryos is normal but *Tbx2* (c,d) and *Tbx3* (e,f, arrowheads) are below normal and expression of the chamber marker *Anf* is expanded (g,h, arrowheads). (B) *In situ* hybridisation at E9.5 on paraffin sections. In E9.5 *Arid3b*$^{gt/gt}$ embryos *Bmp2* expression diminishes (a,b, arrowhead), *Tbx2* and *Tbx3* expression remains low (c-f, arrowheads), and expansion of Anf towards the AVC is more evident (g,h, arrowheads). (C) Expression of *Bmp2* (RNA *in situ* hybridization) and pSmad1/5/8 (immunohistochemistry, red) in consecutive sections at E9.0 (a-d) and E9.5 (e-h). MF20 labelling (immunohistochemistry, green) was used to stain myocardium. No differences between WT and *Arid3b*$^{gt/gt}$ embryos are seen in the myocardium at any stages analysed, but a much lower number of pSmad-positive nuclei is evident in *Arid3b*$^{gt/gt}$ endocardium at E9.5 (g,h, arrowheads), although not at E9.0 (c,d, arrowheads). Scale bars: 250 µm in A; 150 µm in B; 100 µm in C. a, atrium; avc, atrioventricular canal; v, ventricle.

mechanistic insight into *Arid3b* function. One of them, *Bhlhb2*, is a transcription factor of the basic helix-loop-helix family that has been shown to regulate cardiac progenitor cell fate determination downstream of Wnt/β-catenin signalling (Kwon et al., 2009). *Bhlhb2* was one of the most strongly upregulated genes in the microarray analysis, both in E9.0 whole embryos and in E9.5 hearts. *In situ* hybridisation revealed much higher expression in *Arid3b*-null embryos, both in whole-mount specimens (Fig. 5Ca,b,g,h) and in sections (Fig. 5Cc-f,i-l). Strong upregulation was also confirmed by qPCR (supplementary material Fig. S6B,C). Expression was particularly strong in the heart poles, especially in the IFT (Fig. 5Cj,l, arrowheads; compare with d,f). *Bhlhb2* has been shown to negatively regulate *Smyd1*, a histone methyltransferase essential for cardiomyocyte differentiation (Kwon et al., 2009). *Smyd1* expression was reduced in mutant hearts, notably in the IFT, the same area in which *Bhlhb2* was highly expressed (as detected by *in situ* hybridisation, see Fig. 5C, and confirmed by qPCR, supplementary material Fig. S6B,C). This region, which corresponds to a site of high *Arid3b* expression in WT hearts and to the pole-shortening defect in the *Arid3b* mutants, also lacked SMA and TnT expression. Expression of SMA is observed at the heart poles in WT and mutant embryos (Fig. 6Aa-d). However, mutant embryos lack expression in the distal regions closer to the SHF, both in the IFT (at E9.5, Fig. 6Ad) and in the OFT (at E9.0, Fig. 6Af, and at E9.5, Fig. 6Ah), suggesting defective differentiation or delayed maturation of heart progenitors. A similar pattern was observed for TnT, the expression of which was absent in the distal part of the heart poles in the mutant (supplementary material Fig. S9). These results suggest that *Arid3b* regulates cardiac progenitor differentiation at the heart poles indirectly through repression of *Bhlh2*.

The other upregulated gene selected from the microarray analysis was *Lims2* (also known as *Pinch2*), a focal adhesion protein that binds to integrin-linked kinase and modulates its activity. *Lims2* is an adaptor protein linking integrins to the actin cytoskeleton and has been shown to regulate cell shape and migration (Zhang et al., 2002; Boudoukha et al., 2010). *In situ* hybridisation of *Lims2* confirmed clear upregulation in *Arid3b* mutants, again very conspicuous at the heart poles (Fig. 5D, also confirmed by qPCR, see supplementary material Fig. S6B,C). Overexpression of *Lims2 in vitro* impairs cell adhesion and motility (Zhang et al., 2002), similar to observations in *Arid3b*-deficient cells (Casanova et al., 2011), suggesting that its upregulation also contributes to the heart pole defects observed in *Arid3b* mutants.

Development (2014) 141, 4168-4181 doi:10.1242/dev.109918

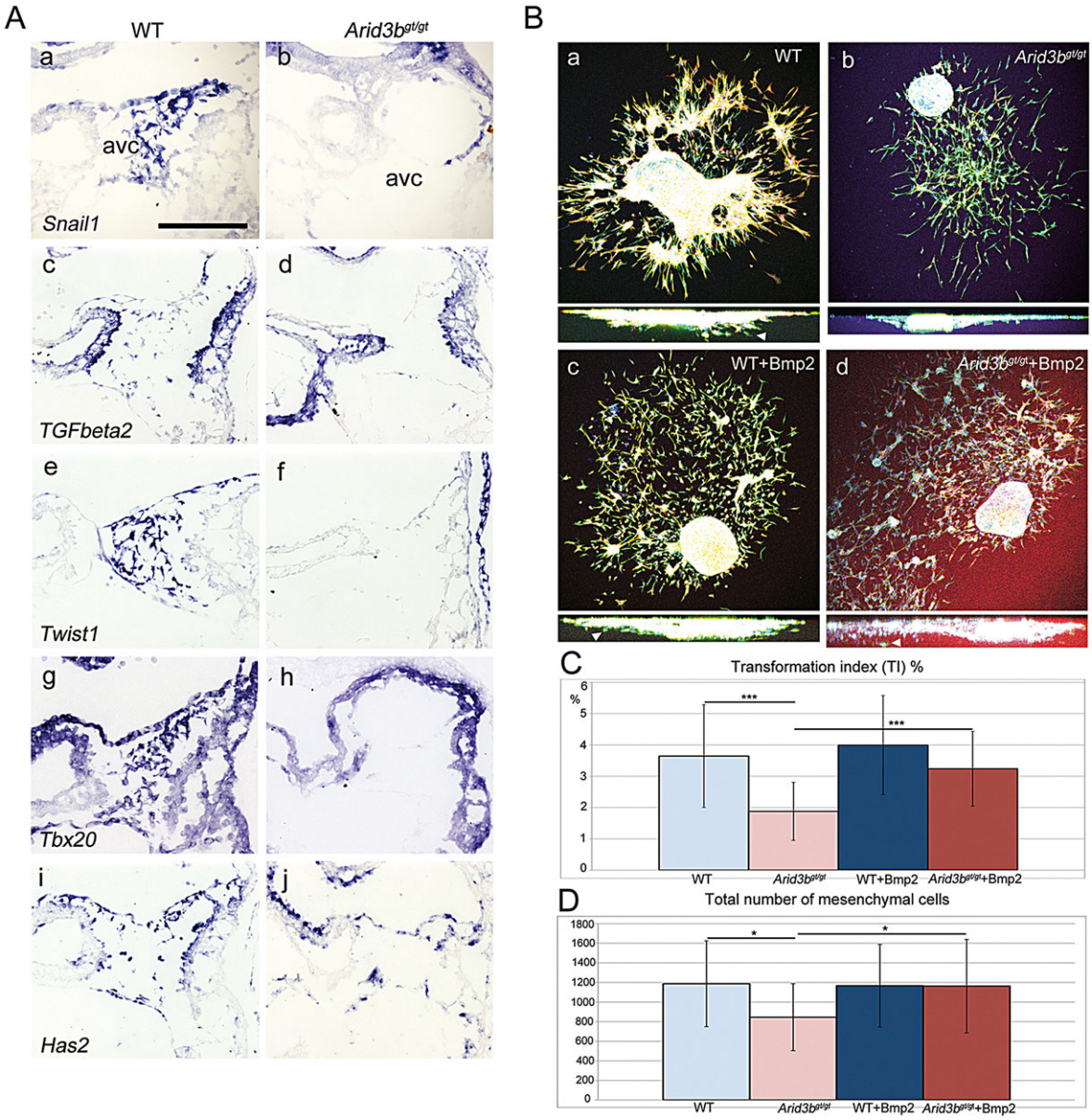

Fig. 4. EMT is defective in *Arid3b* mutant hearts. (A) *In situ* hybridization of molecules involved in EMT in the AVC. Expression levels of *Snai1* (a,b), *Tgfb2* (c,d), *Twist1* (e,f) and *Tbx20* (g,h) are significantly lower in the mutant AVC endocardium, whereas *Has2* (i,j) is unaltered; note also the almost total absence of mesenchymal cells invading the cushions in the mutant. (B) AVC explants on collagen gels stained for SMA (red) and phalloidin (green). Both the total number of mesenchymal cells (scattered cells on top panels) and the proportion of cells invading the gel (arrowheads in bottom panels, *z*-axis) were lower in mutant (b) than in WT (a) explants. After addition of Bmp2, the total number of mesenchymal cells and the transformation index (TI) in mutant explants (d) were restored to the levels in WT explants (c). (C,D) Quantification of the results (TI, in %). Scale bar: 150 µm. Results are mean±s.d. **P*<0.05, ****P*<0.001; Student's *t*-test.

Arid3b deficiency does not affect cell proliferation or cell death of SHF progenitors

To further investigate the cause of the heart pole defects in the absence of *Arid3b*, we analysed cell proliferation and cell death in Islet1+ progenitors in the SHF (and also in the heart tube and the forming heart chambers) between stages E8.0 and E9.5. Wild-type and mutant hearts contained similar total numbers of Islet1+ progenitors and there were no significant differences in proliferation in any region at the stages analysed, as measured by pH3 staining and 5-bromo-2′-deoxyuridine (BrdU) incorporation (SHF analysis in supplementary material Fig. S10A and heart analysis in supplementary material Fig. S11A). Apoptotic cell death assessed by terminal deoxynucleotidyl transferase dUTP nick end labeling (TUNEL) labelling was also similar, except for a significantly higher level in the SHF and atria of mutant hearts at E9.5, which was the only stage at which we detected a reduction in the total number of Islet1+ cells in *Arid3b* mutants (supplementary material Fig. S10B and Fig. S11B).

The level of Isl1 expression in heart progenitors appeared normal in mutant embryos (supplementary material Fig. S10C), as was the expression of other genes reported to regulate SHF cardiac progenitors and normal OFT formation, such as *Fgf8* and *Tbx1* (supplementary material Fig. S10D). Moreover, expression of several genes (*Fgf8*, *Tbx1*, *Shh*) in the pharyngeal endoderm, a tissue important for heart formation where *Arid3b* is also expressed, was similar in mutant as compared with WT embryos (supplementary material Fig. S10E). Notably, accumulation of Islet1+ progenitors was seen in the SHF in the OFT region at E9.5 (Fig. 6Ah, asterisk). Additionally, the actin

Development (2014) 141, 4168-4181 doi:10.1242/dev.109918

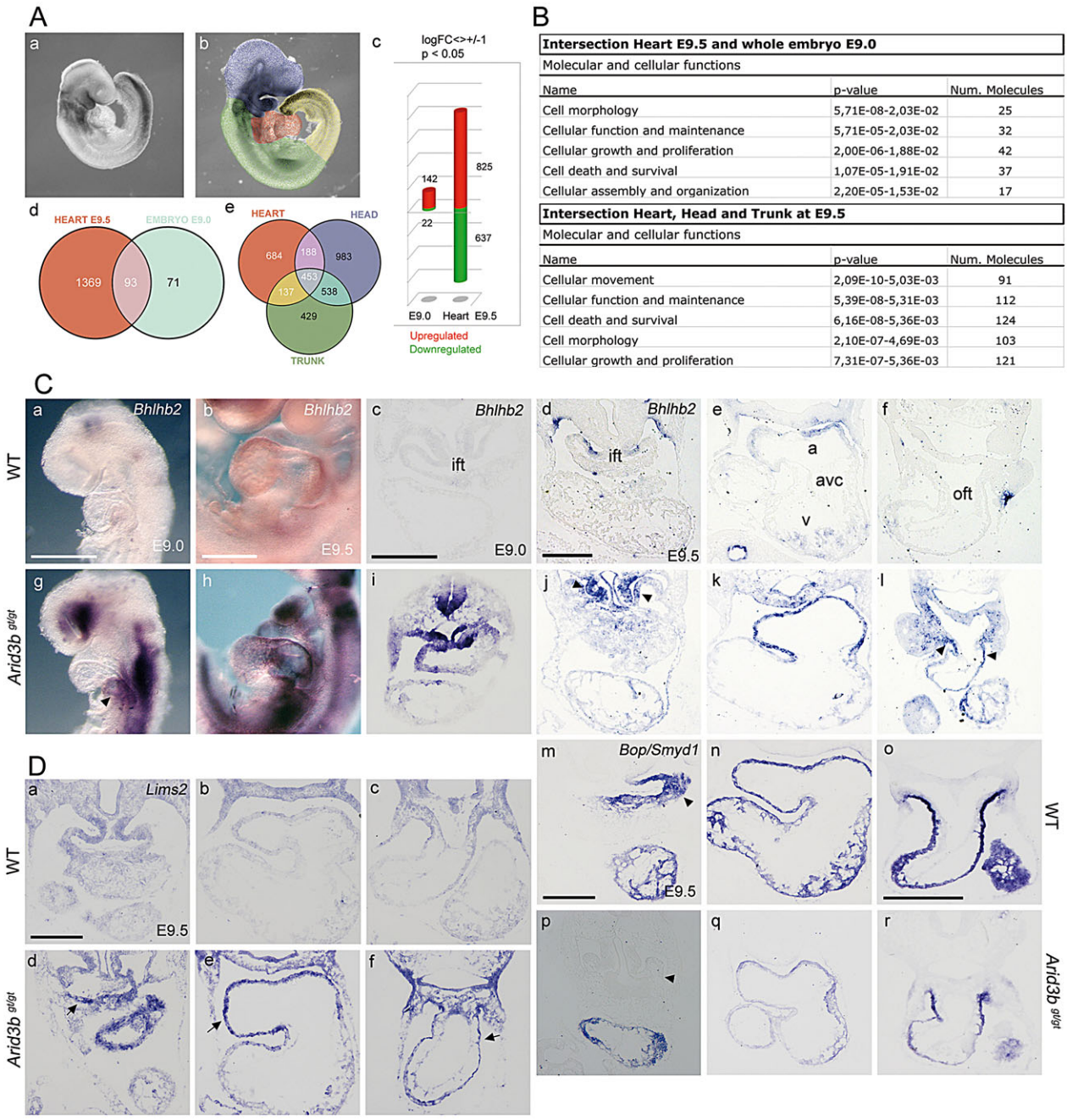

Intersection Heart E9.5 and whole embryo E9.0

Molecular and cellular functions

Name	p-value	Num. Molecules
Cell morphology	5,71E-08-2,03E-02	25
Cellular function and maintenance	5,71E-05-2,03E-02	32
Cellular growth and proliferation	2,00E-06-1,88E-02	42
Cell death and survival	1,07E-05-1,91E-02	37
Cellular assembly and organization	2,20E-05-1,53E-02	17

Intersection Heart, Head and Trunk at E9.5

Molecular and cellular functions

Name	p-value	Num. Molecules
Cellular movement	2,09E-10-5,03E-03	91
Cellular function and maintenance	5,39E-08-5,31E-03	112
Cell death and survival	6,16E-08-5,36E-03	124
Cell morphology	2,10E-07-4,69E-03	103
Cellular growth and proliferation	7,31E-07-5,36E-03	121

Fig. 5. Microarray analysis reveals *Bhlhb2* and LIMS2 as *Arid3b* target genes. (A) (a,b) Samples used for the microarrays. RNA was extracted from whole embryos at E9.0 (a) or from dissected heart, head and trunk regions of E9.5 embryos as shown in colours (b). (c) Microarray analysis, using a twofold-change threshold and an adjusted *P*-value of <0.05 for false discovery rate, identified a total of 164 genes in E.9.0 whole embryos and 1462 genes in E9.5 hearts as differentially expressed between mutant and control embryos (142 and 825 genes upregulated and 22 and 637 genes downregulated, respectively). (d,e) The lists of genes were compared to identify genes similarly altered in the different conditions; 93 were altered in E9.0 whole embryos and E9.5 hearts (d), and 453 genes were altered in all three tissues analysed in E9.5 embryos (e). (B) Ingenuity functional analysis of the commonly differentially expressed genes. The five top functions overrepresented in the 93 and 453 common genes are shown; note that cell morphology and cellular movement are the most overrepresented. (C) RNA *in situ* hybridization of genes regulated by *Arid3b*. Detection of *Bhlhb2* RNA in whole-mount embryos (a,b,g,h) and on paraffin sections (c-f,i-l) at E9.0 and E9.5. High levels of expression in the heart poles are evident in the *Arid3b*$^{gt/gt}$ (g,j,l, arrowheads). *In situ* hybridization of *Bop*/*Smyd1*, a marker for cardiomyocyte differentiation, in WT (m-o) and *Arid3b*$^{gt/gt}$ (p-r) embryos. The overall level of expression is lower in *Arid3b*$^{gt/gt}$ myocardium and OFT and absent in the IFT (m,p, arrowheads). (D) Expression of *Lims2* in WT (P-R) and *Arid3b*$^{gt/gt}$ (V-X) hearts; note the upregulation in the OFT and atria of the mutants (arrows). Scale bars: 200 µm in sections, 500 µm in whole-mount.

cytoskeleton of Islet1+ cells in the SHF and the overall tissue architecture of this region were abnormal in mutants. SHF cells in WT hearts have a wide band of actin on the luminal side (Fig. 6B, WT), which is thicker at the IFT region (Fig. 6Bc), suggestive of a polarized epithelium. By contrast, mutant SHF cells do not show such a clear actin band (Fig. 6Bd). Moreover, cells dorsal to the wall epithelium, which appear loose and mesenchyme-like in the WT (Fig. 6Bg), appear more compact and epithelial-like in the mutant (Fig. 6Bh).

Development (2014) 141, 4168-4181 doi:10.1242/dev.109918

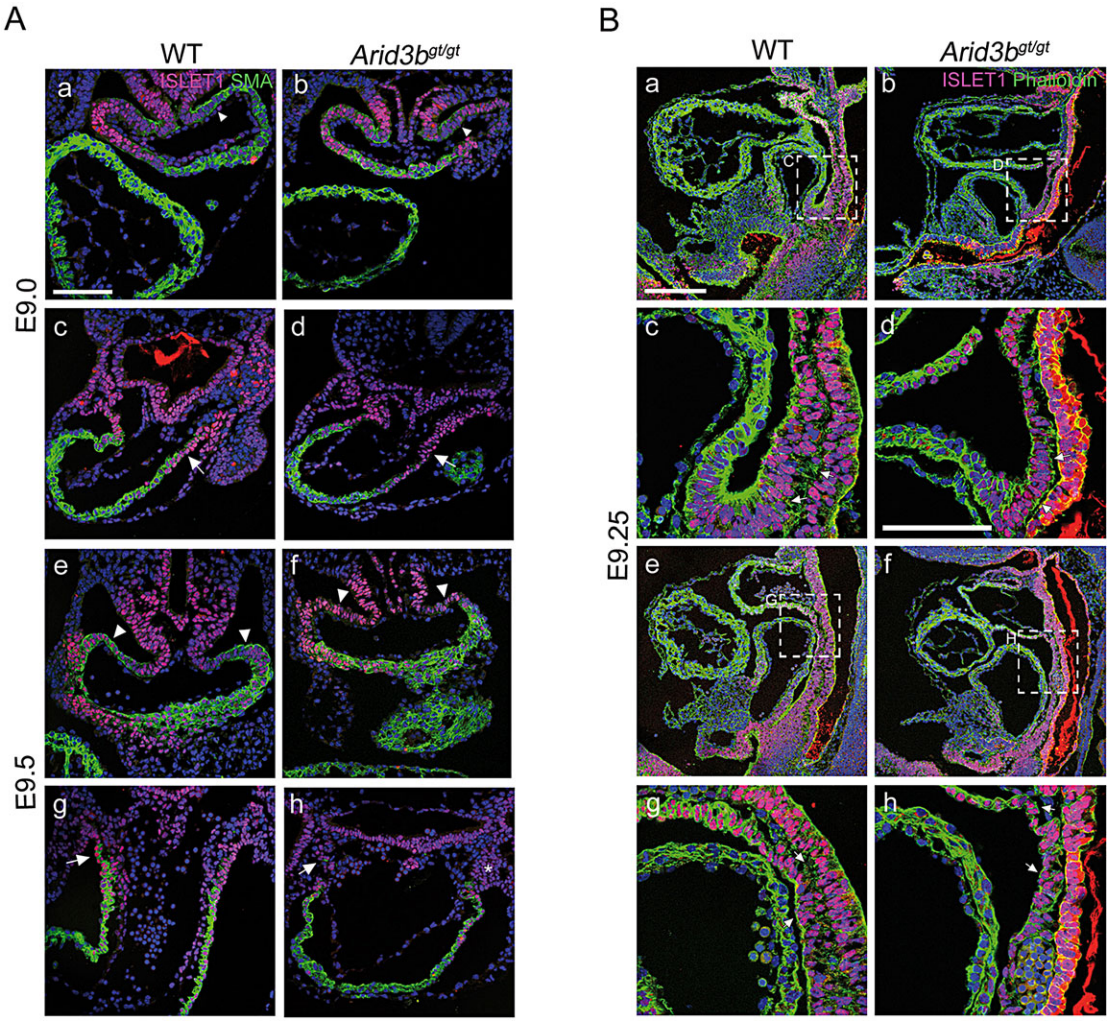

Fig. 6. *Arid3b* mutants lack differentiation of cardiomyocytes in the heart poles and show abnormal SHF architecture. (A) SMA and Islet1 immunostaining on paraffin sections of *Arid3b*$^{gt/gt}$ and WT embryos. Expression of SMA is reduced in the most dorsal part of the OFT at E9.0 and E9.5 (white arrows, compare d with c and h with g). In the IFT, SMA expression in *Arid3b*$^{gt/gt}$ embryos is normal at E9.0, but less-differentiated cells are seen at the dorsal-most region of the sinus horns at E9.5 (white arrowheads). An accumulation of Islet1+ cells can be observed at the entrance of the OFT of *Arid3b*$^{gt/gt}$ embryos (h, asterisk). (B) Phalloidin (green) and Islet1 (red) staining on longitudinal sections in E9.25 embryos. Mutant cells (d,h) appear more compact and epithelial-like than WT cells (c,g, arrows). Furthermore, the actin band facing the pericardial cavity, very conspicuous in WT embryos (g, arrow), is less prominent in the mutant (h). Scale bars: 100 µm in A; 200 µm in Ba,Bb,Be,Bf; 100 µm in Bc,Bd,Bg,Bh.

Taken together, these results suggest that a difference in cell number is not the primary cause of the observed defects in mutant hearts and that *Arid3b* deletion appears not to alter the specification of heart progenitors in the SHF, which nonetheless has abnormal tissue architecture.

Addition of SHF progenitors to the heart poles is impaired in *Arid3b* mutant embryos

The results presented so far show that Islet1+ progenitors are correctly specified in the mutant SHF, that proliferation and cell death are unaltered and that the early patterning of the heart is normal. However, the cellular architecture and tissue organization in the SHF are disrupted and eventually the poles of the heart are malformed. Moreover, *Lims2*, which regulates cell motility, is upregulated in the heart poles of *Arid3b* mutants. This suggests abnormal incorporation of Islet1+ progenitors into the heart, probably due to defective cell movements or cell rearrangements. To directly analyse the fate of mutant SHF cells, we DiI-labelled Islet1+ progenitors, both in ventro-caudal positions at E8.0 (6 ps), which will contribute to the IFT (Fig. 7), and in rostro-lateral positions at E8.5 (10 ps), which will contribute to the OFT and right ventricle (Fig. 8). Cells were labelled, embryos cultured *in vitro* for 24 h and the position of DiI-positive cells was recorded. Labelling of IFT progenitors led to the presence of DiI-positive cells in the IFT in 91% of WT embryos, but in only 48% of *Arid3b* mutant embryos (Fig. 7U). Similarly, labelling of OFT progenitors led to the presence of DiI-positive cells in the proximal OFT in most WT embryos (66%), with a significant proportion showing cells in the right ventricle (13%). By contrast, in most mutant embryos (55%), DiI-positive cells were found in the distal OFT close to the SHF, and only reached the right ventricle in one embryo (5%) (Fig. 8N). This reduced contribution of cells to the IFT and OFT in mutant as compared with WT embryos was statistically significant. Taken together, these results suggest that Islet1+ progenitors, although present in *Arid3b* mutant SHF, have an impaired capacity to contribute to the heart poles, which eventually causes the observed cardiac defects. The results from our microarray analysis offer a possible mechanistic explanation for the defects observed in the mutant embryos.

Development (2014) 141, 4168-4181 doi:10.1242/dev.109918

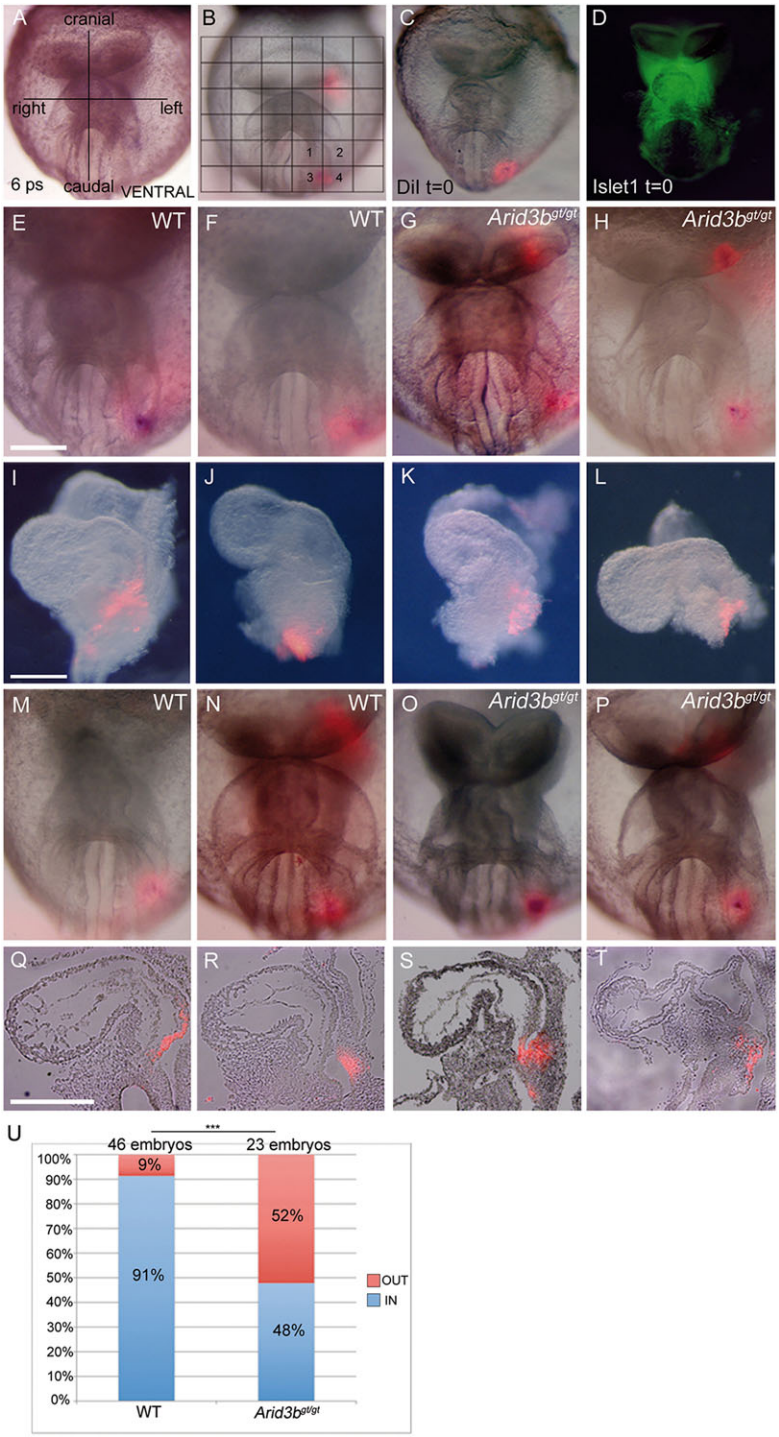

Fig. 7. Addition of Islet1-positive progenitors to the IFT is impaired in *Arid3b*$^{gt/gt}$ embryos. (A) Ventral view of a 6-somite embryo, as used in DiI fate-mapping experiments, showing the left-right and cranial-caudal axes for orientation. (B) Example DiI labelling of the posterior SHF (pSHF) to study the contribution of Islet1+ cells to the IFT. A grid was used to map the position of the injection; for the analysis shown here, positions 3 and 4 (caudo-lateral) were considered. DiI (red fluorescence, B,C) was injected into the region containing Islet1+ cells, later detected by whole-mount immunochemistry (D, green). (E-H) *Arid3b*$^{gt/gt}$ and WT embryos labelled with DiI at similar positions (t=0) and (I-L) the resulting label seen in whole dissected hearts after 24 h of *in vitro* culture. Images show WT (E,F,I,J) and *Arid3b*$^{gt/gt}$ (G,H,K,L) embryos with DiI-labelled cells in the heart IFT (I,K) recorded as 'IN' and those with labelled cells outside the heart (J,L) recorded as 'OUT'. (M-P) Additional examples of DiI labelling in the pSHF at t=0; in this case, 24 h after labelling embryos were cryosectioned and DiI staining observed on longitudinal sections (Q-T). DiI-labelled cells could be detected in the heart IFT in some wild-type (Q) and *Arid3b*$^{gt/gt}$ (S) embryos. In other cases, DiI-labelled cells appear outside the IFT (R, wild type; T, *Arid3b*$^{gt/gt}$). (U) Summary of the contributions of the pSHF to the IFT in normal and *Arid3b*$^{gt/gt}$ embryos expressed as the percentage of embryos with labelling inside or outside of the IFT. A two-sample test for equality of proportions was used to compare the two groups. The percentage of embryos with labelling in the IFT is significantly higher in the WT than the *Arid3b*$^{gt/gt}$ group (***P=0.0001903). Scale bars: 250 µm.

DISCUSSION

Arid3b is essential for mouse embryo development, but its precise functions are not well characterised. Our results show that *Arid3b* is required for heart development during three stages: pole formation, myocardium differentiation and AVC patterning and maturation.

A previous report (Takebe et al., 2006) dismissed a direct role for *Arid3b* in cardiac development on the basis that *Arid3b* expression was barely detected in the developing WT heart and that cardiac muscle and heartbeat were present in *Arid3b* null mutants. The observed cardiovascular defects were attributed to death of neural crest cells and thus a failure in their contribution to the OFT. Here, we show a clear expression of *Arid3b* in cardiac progenitors from early stages of heart development in both the cardiac crescent and in the SHF. Although expression in the chamber myocardium soon regresses, high levels of expression are maintained at the heart poles, areas that do not form properly in *Arid3b* null embryos. The expression pattern and the early appearance of the defects (shortening of the poles, detectable from E9.0 on) strongly suggest a cell-autonomous defect in SHF cardiac progenitors, contrary to what was previously reported.

Although we observed heart beating and circulation in mutant embryos, their vasculature was abnormal: remodelling of the

Development (2014) 141, 4168-4181 doi:10.1242/dev.109918

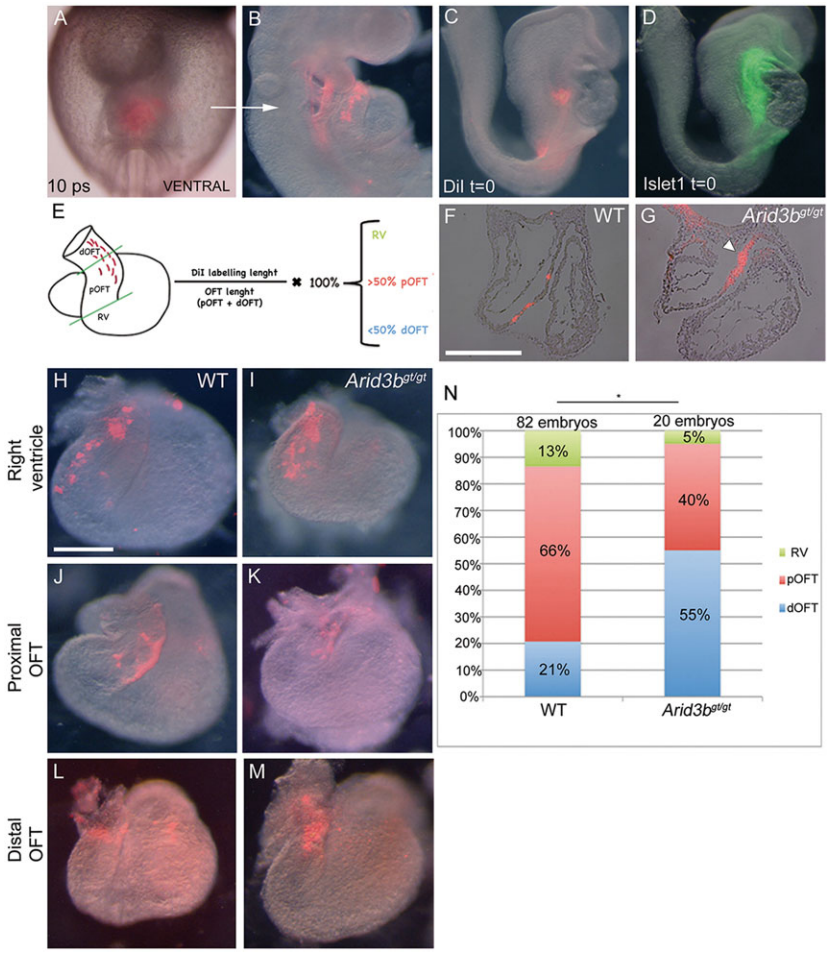

Fig. 8. Contribution of progenitors to the OFT is altered in *Arid3b*$^{gt/gt}$. (A) Ventral view of DiI labelling in a representative embryo at t=0. (B) Lateral view after 24 h *in vitro* culture. (C,D) DiI labelling in an Islet1+ region (D, immunostaining with anti-Islet1 antibody). (E) Scheme illustrating the three regions in which the heart was subdivided for data analysis. (F,G) Cryosections of WT and mutant embryos 24 h after labelling; note the accumulation of DiI-labelled cells at the entrance of the heart in the mutant (arrowhead). (H-M) Examples of the three locations of the DiI staining 24 h after labelling in WT and mutant embryos. (N) Summary of the contributions of the AHF to the heart in *Arid3b*$^{gt/gt}$ and control embryos expressed as the percentage of embryos with labelled cells in each of the regions. Fisher's exact test was used to compare the two groups. The difference in the distribution between WT and *Arid3b*$^{gt/gt}$ embryos is statistically significant (**P*=0.01149). Scale bars: 250 µm.

primitive network in the yolk sac was not accomplished and vessels in the embryo were smaller than in WT embryos. As *Arid3b* is not expressed in the endothelium at early stages, this suggests that defects in vessel maturation are non-autonomous. In fact, *Arid3b* is expressed in the endoderm of the yolk sac, pointing to an indirect role for *Arid3b* in vessel maturation. Later on, *Arid3b* is indeed expressed in the endothelium, suggesting that it has additional roles in the maintenance or physiology of this tissue; however, the early death of mutant embryos prevents studying this possibility. Noteworthy, a genome-wide association study has recently identified eight loci associated with elevated blood pressure and hypertension in patients (Newton-Cheh et al., 2009). Interestingly, *Arid3b* is in the region showing the strongest association with elevated diastolic blood pressure, suggesting a potential role for *Arid3b* in the regulation of adult cardiovascular physiology and in the aetiology of hypertension.

Specification of cardiac precursors and early patterning of the heart tube and chambers are normal in *Arid3b* null embryos. However, Islet1+ progenitors fail to express early myocardial markers (such as SMA and TnT) in the heart poles. Interestingly, *Bhlhb2*, a repressor that inhibits expression of another myocardial marker, *Smyd1* (Kwon et al., 2009), is one of the genes that was most upregulated in mutant embryos in our microarray analysis, indicating that *Arid3b* normally represses *Bhlhb2*. In *Arid3b* mutant embryos, *Smyd1* expression is below-normal throughout the myocardium and is absent in the inflow region, where the higher levels of *Bhlhb2* are observed. As *Smyd1* is necessary for cardiac differentiation and morphogenesis (Gottlieb et al., 2002), its downregulation in *Arid3b* mutants provides a possible molecular explanation for the defect in myocardial differentiation.

Another phenotype of *Arid3b* mutants is the defective AVC patterning. The AVC seems to be properly specified, as early *Bmp2* expression is normal. However, expression of transcription factors that define the AVC (*Tbx2*, *Tbx3*) is markedly impaired from E9.0 on, and this is accompanied by expansion of the chamber marker *Anf*. BMP signal transduction appears to be normal in the myocardium, as pSmad is localised in the nucleus of myocardial cells. This suggests that *Arid3b* functions downstream of pSmad in this tissue and that the defect in *Arid3b* mutants lies in the function of transcriptional complexes that drive the expression of *Tbx2*, a direct target of Bmp2/pSmad signalling (Singh et al., 2009). It is tempting to speculate that Arid3b acts as a coactivator in one of those complexes, perhaps competing with Tbx20, which acts as a repressor of *Tbx2* expression in this context (Singh and Kispert, 2010). Eventually (at E9.5), *Bmp2* expression is also reduced in the mutant myocardium, reflecting the disruption of the maintenance loop between *Bmp2* and *Tbx2*. Moreover, nuclear localization of pSmad in the mutant endocardium, although detected at E9.0, is greatly reduced at E9.5, coinciding with the decrease in myocardial *Bmp2* expression. Myocardium-derived Bmp2 induces EMT in the endocardium, and some EMT markers, such as *Twist1* or *Snai1*, are direct Bmp2 targets (Shelton and Yutzey, 2008; Luna-Zurita et al., 2010). The low expression of *Bmp2* in the *Arid3b* null myocardium could explain the defective EMT observed, a proposition strongly supported by the rescue of EMT in AVC explants *in vitro* by application of Bmp2; this result shows that the defective response of

Development (2014) 141, 4168-4181 doi:10.1242/dev.109918

endocardial cells is not caused directly by the lack of *Arid3b* but is secondary to the patterning defect in the myocardium. This is consistent with the expression of *Arid3b* in the myocardium and its absence in endocardial cells at E9.5, when EMT takes place. However, an autonomous role for Arid3b in the endocardium cannot be completely ruled out, as *Arid3b* could be expressed at a functional level that is below the level of detection by *in situ* hybridization. Moreover, we cannot exclude a later role for *Arid3b* in the endocardium either, as *Arid3b* is robustly expressed in this tissue from E10.5.

A major defect in *Arid3b* mutant embryos is the shortening and abnormal morphology of the heart poles. We could not detect alterations in cell proliferation or cell death of cardiac progenitors in the SHF (increased apoptosis is seen only at E9.5, particularly in the IFT, where the phenotype is usually more severe than in the OFT). These results suggest that the cause of the malformation is not the number of heart progenitors. Moreover, expression of several genes in the pharyngeal endoderm that have been shown to be important for heart formation (*Fgf8*, *Tbx1*, *Shh*) was also normal in *Arid3b* mutants, suggesting that they are not responsible for the cardiac defects. The abnormal morphology and tissue organization of SHF cells in *Arid3b* null embryos is particularly interesting. It is reminiscent of the defects seen in *dishevelled* (Sinha et al., 2012) and other planar cell polarity mutants, such as *Wnt11* knockout mice (Zhou et al., 2007; Cohen et al., 2012), which also show cardiac malformations, especially in OFT development. Moreover, the altered actin cytoskeleton in *Arid3b* mutant cells is consistent with the regulation by *Arid3b* of cell motility *in vitro* and *in vivo* (Casanova et al., 2011). Together, these data suggest that *Arid3b* is required for proper deployment of cardiac progenitors to the heart, which fits with the observed accumulation of Islet1+ cells in the SHF next to the OFT. The DiI fate-mapping experiments confirm a defect in the contribution of SHF progenitors to the heart in *Arid3b* mutant embryos. Although the precise cellular mechanisms by which cells are incorporated into the heart (e.g. active migration, cell intercalation, oriented cell division) are not completely understood, regulation of these processes appear to require *Arid3b*. Interestingly, the functional analysis of differentially expressed genes in mutant and WT embryos shows that cell morphology and cellular movement are the most overrepresented pathways. Moreover, one of the most upregulated genes in the mutant hearts is *Lims2*, a component of integrin-linked kinase complex. Overexpression of this gene has been shown to alter cell adhesion and cell motility (Zhang et al., 2002; Boudoukha et al., 2010), making it a likely candidate mediator of *Arid3b* effects.

Our results show that *Arid3b* has a previously unnoticed, direct role in cardiac development, regulating the shape, movements and differentiation of heart progenitors. This establishes *Arid3b* as a candidate regulator of human heart development and cardiovascular physiology, and it would be important to establish the relevance of human *ARID3B* mutations in congenital heart disease and hypertension.

MATERIALS AND METHODS

Ethics statement

All animal work has been performed according to the guidelines of the Committee on Ethics and Animal Welfare established at CNIC, in accordance to Spanish and European laws. The CNIC Committee on Ethics and Animal Welfare has approved this study.

Embryos

Mouse embryos were collected at the indicated gestational stages, with E0.5 defined as noon on the day on which a vaginal plug was detected. For a more precise staging, pairs of somites (ps) were counted and groups were assigned as follows: E8.5 (8-12 ps), E9.0 (13-16 ps), E9.25 (17-23 ps), E9.5 (24-26 ps). Embryos were dissected in cold PBS and fixed overnight in 4% PFA at 4°C.

Mouse gene-trap model and *Arid3b* mutants

A mouse line (CD1;129P2-*Arid3b*$^{Gt(RRJ028)Byg}$) was generated as previously described (Casanova et al., 2011) from a Baygenomics gene-trap ESC line (http://www.genetrap.org/cgi-bin/annotation.py?cellline=RRJ028), which has an insertion of the vector pGT0lxf in the intron after the first coding exon of *Arid3b*. This produces a fusion protein containing the β-galactosidase (β-Gal) enzyme but lacking all the functional domains of *Arid3b*. Adult mice were genotyped by PCR based on amplification of the first *Arid3b* exon (WT and heterozygous) and the presence of the β-Geo cassette in the gene-trap vector (heterozygous). Mutant (referred to as *Arid3b*$^{gt/gt}$ or *Arid3b*-null) embryos were obtained by mating heterozygous animals. Embryos were genotyped according to β-Gal activity, measured as the different intensity of staining due to different *lacZ* expression levels. Heterozygous mice were viable and fertile, and both wild-type and heterozygous embryos were used as controls; for simplicity, we always use the term wild type for the control.

β-galactosidase staining

Embryos were dissected and fixed with 0.125% glutaraldehyde. β-galactosidase staining was performed in whole embryos or tails with X-Gal as substrate, as previously described (Stoykova et al., 1998).

Histology and immunochemistry

Embryos were collected and fixed in 4% PFA overnight at 4°C, dehydrated and embedded in paraffin. Alternatively, embryos were included in gelatine-sucrose and frozen for cryostat sectioning. For histological analysis, 5 µm paraffin sections were stained with haematoxylin and eosin (H&E) using a standard protocol. For immunochemistry on 5 µm paraffin sections, slides were hydrated and antigens retrieved by microwave heating for 15 minutes in 10 mM citrate buffer, pH 6.0. Sections were incubated overnight at 4°C with primary antibodies against: Islet1 (Hybridoma Bank, clone 39.4D5; 1:100), SMA-Cy3 (Sigma, C6198; 1:100), troponin T (Hybridoma Bank, clone CT3; 1:200), myosin heavy chain MF20 (Hybridoma Bank, clone MF20; 1:20) and phospho-SMAD 1/5/8 (Cell Signaling, 9511; 1:200). Slides were incubated with the following secondary antibodies for 1 h at room temperature: anti-mouse biotin (Jackson ImmunoResearch, 115-066-071; 1:500), HRP-goat anti-rabbit (Dako, P0448; 1:100). Slides were then incubated either with streptavidin-Alexa 488 (Invitrogen, s-11223; 1:500) or streptavidin-DyLight 594 (Jackson ImmunoResearch, 016-510-084; 1:500), or revealed with the TSA Fluorescence System (PerkinElmer, NEL744001KT). Alternatively, 8 µm cryostat sections were used with primary anti-CD31 antibodies (BD Biosciences, 553370; 1:50) or β-galactosidase (Hybridoma Bank, clone 40-1a; 1:10). For actin staining Alexa 488-conjugated phalloidin (Molecular Probes, A12397; 1:200) was used on frozen sections. Slides were mounted with Vectashield containing DAPI. Images were acquired on a Leica TCS SP-5 confocal microscope.

RNA *in situ* hybridisation in whole-mount embryos and on paraffin sections

Whole-mount *in situ* hybridisation was performed as previously described (Wilkinson and Nieto, 1993). *In situ* hybridisation on sections (7 µm) was performed in paraffin-embedded embryos according to previously described protocols with some modifications (Kanzler et al., 1998). Images were acquired with a Nikon Eclipse 90i microscope and in a Leica MZ-12 dissecting microscope. Details of the probes used are provided in supplementary material Table S8.

Proliferation and cell death

Cell death was detected using a TUNEL kit (Roche, *In Situ* Apoptosis Detection Kit – Fluorescein). Cell proliferation was measured by anti-phospho-Histone3 labelling (Millipore, 06-570; 1:200) on paraffin sections

Development (2014) 141, 4168-4181 doi:10.1242/dev.109918

as described above. For BrdU staining, embryos at E8.5 were dissected and incubated in culture medium (DMEM, 10% FBS) with 10 mg/ml BrdU for 1 h at 37°C and 5% CO_2. Embryos were quickly transferred to ice-cold PBS to quench BrdU incorporation and were fixed overnight in 4% PFA at 4°C. Embryos were embedded in paraffin and immunostaining was performed as described above with anti-BrdU antibody (BD Biosciences, 7580; 1:30). The total number of nuclei (DAPI staining) and BrdU-positive, PH3-positive and TUNEL-positive cells were counted on 9-20 sections from at least three different embryos per condition. Islet1 was used as a marker of the SHF population. Statistical analysis was performed using a two-tailed unpaired Student's *t*-test.

Ink injection

Indian Ink was injected following a modified version of a previously described protocol (Winnier et al., 1999). Embryos at stage E9.25 were dissected in warm culture medium (DMEM, 10% FBS) and Pelikan Indian Ink diluted 1:40 in PBS was injected into the left ventricle. Embryos were fixed in 4% PFA overnight and dehydrated with methanol. To visualise the ink, embryos were cleared for several hours in benzyl benzoate/benzyl alcohol (vol. 2:1).

Length measurement in OFT and IFT regions

For the quantification of the length of the poles of the heart, pictures of the right side (for OFT) or left side (for IFT) of embryos at E9 and E9.5 were analysed using ImageJ software. Lines were manually draw marking the contour of the inner curvature of the OFT up to the start of the right ventricle or the outer curvature of the IFT up to the start of the left ventricle and the length was measured.

For measuring the IFT length we used 12 wild-type and 15 mutant embryos at stage E9.0, and 10 wild-type and 13 *Arid3b*-null embryos at stage E9.5. For measuring the length of OFT, 12 wild-type and 17 $Arid3b^{gt/gt}$ embryos were used at stage E9.0, and 12 wild-type and 12 mutant embryos at stage E9.5.

AVC explants

AVC explants were prepared as described previously (Luna-Zurita et al., 2010). A 1.5 mg/ml solution of rat-tail collagen type I (BD Bioscience) was prepared and allowed to solidify on 4-well micro culture dishes at 37°C and 5% CO_2. Gels were washed several times with DMEM containing 10% FBS, antibiotics, antimycotic (Fungizone, Gibco) and non-essential amino acids, and were left for at least 4 h in the same medium supplemented with 1% insulin-transferrin-selenium (ITS; Gibco). Hearts from E9.5 embryos were dissected in the same medium and AVCs were isolated, cut and placed with the endocardium facing the collagen gel. Explants were left to attach overnight at 37°C and 5% CO_2. Complete medium was added and explants were left to grow for three days. Explants were fixed with 4% PFA for 30 min at room temperature and stained with phalloidin-Alexa 488 (1:100, Molecular Probes) to reveal the actin cytoskeleton and with anti-SMA-Cy3 (1:80, Sigma) to detect mesenchymal cells. Explants were mounted with Vectashield medium containing DAPI to stain the nuclei. For treatment of explants with Bmp2, collagen gels were incubated 30 min before explant culture in medium containing 500 ng/ml recombinant human Bmp2 (R&D Biosciences) and the medium added to attached explants was supplemented with the same concentration of Bmp2. Two-dimensional migration (number of scattered cells) was counted with Imaris software. Three-dimensional migration (number of cells invading the gel) was determined by counting DAPI stained cells in the *z*-stack using ImageJ (NIH). At least 17 explants were considered per condition.

Real-time quantitative PCR

To perform qRT-PCR, total RNA was extracted from hearts. Embryonic hearts at stage E9.5 were dissected in cold PBS in two regions: the first containing the OFT with the pharyngeal endoderm and mesoderm located beneath (OFT), and the second consisting of atria, AVC, ventricle and IFT (chambers). The dissected hearts were stored at –80°C until RNA extraction. Four pools of five mutant or five wild-type embryos were used. RNA was isolated with a Direct-zol RNA MiniPrep Kit (Zymo Research, R2052). cDNA was synthesised with a High Capacity cDNA Transcription Kit (Applied Biosystems, 4368814). qRT-PCR was performed on a 7900HT Fast Real-Time PCR System (Applied Biosystems, 4329001), using *β-actin* and *GAPDH* as normalising genes. Details of the primers used are provided in supplementary material Table S9.

DiI labelling and embryo culture

DiI labelling and embryo culture were performed as described previously (Franco et al., 2001; Dominguez et al., 2012). Embryos ranging from 4 to 11 somites were dissected in Hank's solution without damaging the yolk sac. A long-chain carbocyanine dye (DiI, Molecular Probes) was dissolved in pure ethanol and diluted 1:9 in 0.3 M sucrose containing 0.1% Nile Blue Sulfate after heating at 42°C for 10 min. To track the contribution to the inflow region embryos with 4-7 pairs of somites were injected in a caudal position within the left lateral mesenchyme positive for Islet1 (posterior SHF). The position was determined by using a grid centred on the midline of the embryo. To track the contribution to the OFT embryos from 8 to 11 somites were injected beneath the heart tube in a rostral Islet1+ region (AHF). The time of injection was considered t=0. Labelled embryos were photographed under a Leica MZ12F dissecting microscope fitted with a fluorescent lamp and cultured in rolling bottles for 24 h in 75% rat serum (Harlan, SR-0100D) and 25% DMEM. For the first 12 h, a 5% CO_2, 5% O_2, 90% N_2 mixture was used; from then on, a 5% CO_2, 20% O_2, 75% N_2 mixture was employed. Two embryos were cultured per bottle, and were distinguished by DiI injection into the head (embryo 2) or without dye (embryo 1). After 24 h in culture embryos were collected in PBS, the yolk sac was removed and embryos were fixed in 4% PFA overnight at 4°C. From the total number of labelled embryos, 51 were excluded due to abnormal development. We also excluded 70 embryos due to inappropriate labelling (cases that presented leakage of DiI into the pericardial cavity or the heart lumen during injection, and cases when labelling was too deep and DiI appeared mostly in the pharyngeal endoderm but not in the heart OFT). A total of 43 wild-type embryos and 23 *Arid3b*-null embryos were considered for the analysis of embryos marked for IFT contribution, and a total of 82 wild-type embryos and 20 *Arid3b*-null embryos were analysed in the case of embryos labelled for OFT contribution. The contribution to the IFT was measured by determining whether DiI-labelled cells were observed inside or outside of the heart tube (binomial distribution). The contribution to the OFT was classified into three regions: the length of the OFT was measured by ImageJ and divided into an upper half (distal OFT) and a lower half (proximal OFT). The third region was the right ventricle, defined by using the outer curvature of the heart tube. Employing R, a two-sample test for equality of proportions with continuity correction was used to analyse the results of pSHF labelling, and Fisher's exact test was used to analyse the contribution to the OFT.

Whole-mount immunochemistry

Embryos were dissected in warm Hank's medium and marked with DiI, and images were acquired as described above. Embryos were fixed immediately in 4% PFA overnight at 4°C. The next day they were dehydrated with methanol and left overnight at –20°C. Whole-mount immunochemistry was performed according to standard protocols. Embryos were rehydrated, permeabilised with 0.5% Triton X-100 (Sigma), left 1 h in blocking solution and incubated overnight at 4°C with anti-Islet1 antibody (Hybridoma Bank, clone 39.4D5; 1:100). Over the next two days embryos were washed in PBT four times and incubated overnight, first with biotin Sp anti-mouse IgG (Jackson ImmunoResearch; 1:500) and then with streptavidin-Alexa 488 (Invitrogen; 1:500). Embryos were stored in Vectashield and images were acquired under a Leica fluorescent microscope.

DNA microarray

E9.5 embryos were dissected in cold PBS. Three different regions were separated: head (including head and first branchial arch); heart (including the heart tube and the pharyngeal mesoderm and endoderm located beneath); and trunk (including the body from the otic vesicle to somite 15). Four wild-type and four mutant embryos were collected for each of the microarray triplicates. For the E9.0 whole-embryo microarray, four wild-type and four mutant samples, consisting of 3-4 embryos each, were used. RNA was

extracted with a Qiagen extraction kit and RNA quality was checked using a Nanodrop spectrophotometer measure and gel electrophoresis. Samples were labelled and hybridised to Agilent chips (Whole Mouse Genome Microarray 4 x 44K, G4122F and G4846A, Agilent Technologies). A functional analysis was performed with the Ingenuity Pathway Analysis software (Ingenuity Systems). Details of the microarray protocols are provided in the supplementary materials and methods. The data for the microarrays have been deposited in NCBI's Gene Expression Omnibus and are accessible through GEO Series accession number GSE62072.

Acknowledgements
We would like to thank M. A. Nieto and M. Ros for probes, M. Manzanares and M. Torres for critically reading the manuscript and S. Bartlett for language editing.

Competing interests
The authors declare no competing financial interests.

Author contributions
V.U. and J.J.S.-E. designed the study, analysed the data, discussed the results and wrote the manuscript. V.U. performed most experiments, with the help of C.B.-C. (histology and *in situ* hybridisation) and J.C.C. (AVC explants and *in situ* hybridisation). J.N.D. advised on DiI labelling. J.L.d.l.P. provided probes, reagents and advised on AVC explants. J.J.S.-E. supervised the whole project.

Funding
This work was supported by the Spanish Ministerio de Ciencia e Innovación, the Instituto de Salud Carlos III and the Fundación La Marató TV3 [grants BFU2006-12859, CP07/00251 and 082030, respectively, to J.J.S.-E.]. V.U. and J.C.C. were supported by FPU fellowships from the Spanish Ministerio de Educación. The CNIC is supported by the Spanish Ministerio de Economía y Competitividad and by the Pro-CNIC foundation.

Supplementary material
Supplementary material available online at
http://dev.biologists.org/lookup/suppl/doi:10.1242/dev.109918/-/DC1

References
Akhavantabasi, S., Sapmaz, A., Tuna, S. and Erson-Bensan, A. E. (2012). miR-125b targets ARID3B in breast cancer cells. *Cell Struct. Funct.* **37**, 27-38.
Black, B. L. (2007). Transcriptional pathways in second heart field development. *Semin. Cell Dev. Biol.* **18**, 67-76.
Boudoukha, S., Cuvellier, S. and Polesskaya, A. (2010). Role of the RNA-binding protein IMP-2 in muscle cell motility. *Mol. Cell. Biol.* **30**, 5710-5725.
Bruneau, B. G. (2013). Signaling and transcriptional networks in heart development and regeneration. *Cold Spring Harb. Perspect. Biol.* **5**, a008292.
Buckingham, M., Meilhac, S. and Zaffran, S. (2005). Building the mammalian heart from two sources of myocardial cells. *Nat. Rev. Genet.* **6**, 826-837.
Casanova, J. C., Uribe, V., Badia-Careaga, C., Giovinazzo, G., Torres, M. and Sanz-Ezquerro, J. J. (2011). Apical ectodermal ridge morphogenesis in limb development is controlled by Arid3b-mediated regulation of cell movements. *Development* **138**, 1195-1205.
Cohen, E. D., Miller, M. F., Wang, Z., Moon, R. T. and Morrisey, E. E. (2012). Wnt5a and Wnt11 are essential for second heart field progenitor development. *Development* **139**, 1931-1940.
Cowden Dahl, K. D., Dahl, R., Kruichak, J. N. and Hudson, L. G. (2009). The epidermal growth factor receptor responsive miR-125a represses mesenchymal morphology in ovarian cancer cells. *Neoplasia* **11**, 1208-1215.
Dominguez, J. N., Meilhac, S. M., Bland, Y. S., Buckingham, M. E. and Brown, N. A. (2012). Asymmetric fate of the posterior part of the second heart field results in unexpected left/right contributions to both poles of the heart. *Circ. Res.* **111**, 1323-1335.
Fahed, A. C., Gelb, B. D., Seidman, J. G. and Seidman, C. E. (2013). Genetics of congenital heart disease: the glass half empty. *Circ. Res.* **112**, 707-720.
Franco, D., Kelly, R., Moorman, A. F. M., Lamers, W. H., Buckingham, M. and Brown, N. A. (2001). MLC3F transgene expression in iv mutant mice reveals the importance of left-right signalling pathways for the acquisition of left and right atrial but not ventricular compartment identity. *Dev. Dyn.* **221**, 206-215.
Gottlieb, P. D., Pierce, S. A., Sims, R. J., Yamagishi, H., Weihe, E. K., Harriss, J. V., Maika, S. D., Kuziel, W. A., King, H. L., Olson, E. N. et al. (2002). Bop encodes a muscle-restricted protein containing MYND and SET domains and is essential for cardiac differentiation and morphogenesis. *Nat. Genet.* **31**, 25-32.
Kanzler, B., Kuschert, S. J., Liu, Y. H. and Mallo, M. (1998). Hoxa-2 restricts the chondrogenic domain and inhibits bone formation during development of the branchial area. *Development* **125**, 2587-2597.
Kelly, R. G. (2012). The second heart field. *Curr. Top. Dev. Biol.* **100**, 33-65.
Kobayashi, K., Era, T., Takebe, A., Jakt, L. M. and Nishikawa, S.-I. (2006). ARID3B induces malignant transformation of mouse embryonic fibroblasts and is strongly associated with malignant neuroblastoma. *Cancer Res.* **66**, 8331-8336.
Kobayashi, K., Jakt, L. M. and Nishikawa, S.-I. (2013). Epigenetic regulation of the neuroblastoma genes, Arid3b and Mycn. *Oncogene* **32**, 2640-2648.
Kortschak, R. D., Tucker, P. W. and Saint, R. (2000). ARID proteins come in from the desert. *Trends Biochem. Sci.* **25**, 294-299.
Kwon, C., Qian, L., Cheng, P., Nigam, V., Arnold, J. and Srivastava, D. (2009). A regulatory pathway involving Notch1/beta-catenin/Isl1 determines cardiac progenitor cell fate. *Nat. Cell Biol.* **11**, 951-957.
Luna-Zurita, L., Prados, B., Grego-Bessa, J., Luxán, G., del Monte, G., Benguría, A., Adams, R. H., Pérez-Pomares, J. M. and de la Pompa, J. L. (2010). Integration of a Notch-dependent mesenchymal gene program and Bmp2-driven cell invasiveness regulates murine cardiac valve formation. *J. Clin. Invest.* **120**, 3493-3507.
Ma, L., Lu, M.-F., Schwartz, R. J. and Martin, J. F. (2005). Bmp2 is essential for cardiac cushion epithelial-mesenchymal transition and myocardial patterning. *Development* **132**, 5601-5611.
Miquerol, L. and Kelly, R. G. (2013). Organogenesis of the vertebrate heart. *Wiley Interdiscip. Rev. Dev. Biol.* **2**, 17-29.
Nagl, N. G., Jr., Wang, X., Patsialou, A., Van Scoy, M. and Moran, E. (2007). Distinct mammalian SWI/SNF chromatin remodeling complexes with opposing roles in cell-cycle control. *EMBO J.* **26**, 752-763.
Newton-Cheh, C. Johnson, T. Gateva, V. Tobin, M. D. Bochud, M. Coin, L. Najjar, S. S. Zhao, J. H. Heath, S. C. Eyheramendy, S. et al. (2009). Genome-wide association study identifies eight loci associated with blood pressure. *Nat. Genet.* **41**, 666-676.
Numata, S., Claudio, P. P., Dean, C., Giordano, A. and Croce, C. M. (1999). Bdp, a new member of a family of DNA-binding proteins, associates with the retinoblastoma gene product. *Cancer Res.* **59**, 3741-3747.
Peng, J. C., Valouev, V., Swigut, T., Zhang, J., Zhao, Y., Sidow, A. and Wysocka, J. (2009). Jarid2/Jumonji coordinates control of PRC2 enzymatic activity and target gene occupancy in pluripotent cells. *Cell* **139**, 1290-1302.
Rana, M. S., Christoffels, V. M. and Moorman, A. F. M. (2013). A molecular and genetic outline of cardiac morphogenesis. *Acta Physiol.* **207**, 588-615.
Rochais, F., Mesbah, K. and Kelly, R. G. (2009). Signaling pathways controlling second heart field development. *Circ. Res.* **104**, 933-942.
Rutenberg, J. B., Fischer, A., Jia, H., Gessler, M., Zhong, T. P. and Mercola, M. (2006). Developmental patterning of the cardiac atrioventricular canal by Notch and Hairy-related transcription factors. *Development* **133**, 4381-4390.
Shandala, T., Kortschak, R. D. and Saint, R. (2002). The Drosophila retained/dead ringer gene and ARID gene family function during development. *Int. J. Dev. Biol.* **46**, 423-430.
Shelton, E. L. and Yutzey, K. E. (2008). Twist1 function in endocardial cushion cell proliferation, migration, and differentiation during heart valve development. *Dev. Biol.* **317**, 282-295.
Singh, R. and Kispert, A. (2010). Tbx20, Smads, and the atrioventricular canal. *Trends Cardiovasc. Med.* **20**, 109-114.
Singh, R., Horsthuis, T., Farin, H. F., Grieskamp, T., Norden, J., Petry, M., Wakker, V., Moorman, A. F. M., Christoffels, V. M. and Kispert, A. (2009). Tbx20 interacts with smads to confine tbx2 expression to the atrioventricular canal. *Circ. Res.* **105**, 442-452.
Singh, R., Hoogaars, W. M., Barnett, P., Grieskamp, T., Rana, M. S., Buermans, H., Farin, H. F., Petry, M., Heallen, T., Martin, J. F. et al. (2012). Tbx2 and Tbx3 induce atrioventricular myocardial development and endocardial cushion formation. *Cell. Mol. Life Sci.* **69**, 1377-1389.
Sinha, T., Wang, B., Evans, S., Wynshaw-Boris, A. and Wang, J. (2012). Disheveled mediated planar cell polarity signaling is required in the second heart field lineage for outflow tract morphogenesis. *Dev. Biol.* **370**, 135-144.
Stoykova, A., Chowdhury, K., Bonaldo, P., Torres, M. and Gruss, P. (1998). Gene trap expression and mutational analysis for genes involved in the development of the mammalian nervous system. *Dev. Dyn.* **212**, 198-213.
Sugi, Y., Yamamura, H., Okagawa, H. and Markwald, R. R. (2004). Bone morphogenetic protein-2 can mediate myocardial regulation of atrioventricular cushion mesenchymal cell formation in mice. *Dev. Biol.* **269**, 505-518.
Takebe, A., Era, T., Okada, M., Martin Jakt, L., Kuroda, Y. and Nishikawa, S.-I. (2006). Microarray analysis of PDGFR alpha+ populations in ES cell differentiation culture identifies genes involved in differentiation of mesoderm and mesenchyme including ARID3b that is essential for development of embryonic mesenchymal cells. *Dev. Biol.* **293**, 25-37.
Valentine, S. A., Chen, G., Shandala, T., Fernandez, J., Mische, S., Saint, R. and Courey, A. J. (1998). Dorsal-mediated repression requires the formation of a multiprotein repression complex at the ventral silencer. *Mol. Cell. Biol.* **18**, 6584-6594.
van den Berg, G., Abu-Issa, R., de Boer, B. A., Hutson, M. R., de Boer, P. A. J., Soufan, A. T., Ruijter, J. M., Kirby, M. L., van den Hoff, M. J. B. and Moorman, A. F. M. (2009). A caudal proliferating growth center contributes to both poles of the forming heart tube. *Circ. Res.* **104**, 179-188.

Development (2014) 141, 4168-4181 doi:10.1242/dev.109918

Vincent, S. D. and Buckingham, M. E. (2010). How to make a heart: the origin and regulation of cardiac progenitor cells. *Curr. Top. Dev. Biol.* **90**, 1-41.

von Gise, A. and Pu, W. T. (2012). Endocardial and epicardial epithelial to mesenchymal transitions in heart development and disease. *Circ. Res.* **110**, 1628-1645.

Waldo, K. L., Hutson, M. R., Ward, C. C., Zdanowicz, M., Stadt, H. A., Kumiski, D., Abu-Issa, R. and Kirby, M. L. (2005). Secondary heart field contributes myocardium and smooth muscle to the arterial pole of the developing heart. *Dev. Biol.* **281**, 78-90.

Wilkinson, D. G. and Nieto, M. A. (1993). Detection of messenger RNA by in situ hybridization to tissue sections and whole mounts. *Methods Enzymol.* **225**, 361-373.

Wilsker, D., Patsialou, A., Dallas, P. B. and Moran, E. (2002). ARID proteins: a diverse family of DNA binding proteins implicated in the control of cell growth, differentiation, and development. *Cell Growth Differ.* **13**, 95-106.

Wilsker, D., Probst, L., Wain, H. M., Maltais, L., Tucker, P. W. and Moran, E. (2005). Nomenclature of the ARID family of DNA-binding proteins. *Genomics* **86**, 242-251.

Winnier, G. E., Kume, T., Deng, K., Rogers, R., Bundy, J., Raines, C., Walter, M. A., Hogan, B. L. and Conway, S. J. (1999). Roles for the winged helix transcription factors MF1 and MFH1 in cardiovascular development revealed by nonallelic noncomplementation of null alleles. *Dev. Biol.* **213**, 418-431.

Zhang, Y., Chen, K., Guo, L. and Wu, C. (2002). Characterization of PINCH-2, a new focal adhesion protein that regulates the PINCH-1-ILK interaction, cell spreading, and migration. *J. Biol. Chem.* **277**, 38328-38338.

Zhou, W., Lin, L., Majumdar, A., Li, X., Zhang, X., Liu, W., Etheridge, L., Shi, Y., Martin, J., Van de Ven, W. et al. (2007). Modulation of morphogenesis by noncanonical Wnt signaling requires ATF/CREB family-mediated transcriptional activation of TGFbeta2. *Nat. Genet.* **39**, 1225-1234.